Theor Chem Acc (2007) 118:443–448
DOI 10.1007/s00214-007-0283-9

REGULAR ARTICLE

Free volume from molecular dynamics simulations and its relationships to the positron annihilation lifetime spectroscopy

Dušan Račko · Riccardo Chelli · Gianni Cardini · Salvatore Califano · Josef Bartoš

Received: 9 January 2007 / Accepted: 14 March 2007 / Published online: 21 April 2007

Abstract The free volume micro-structural properties of propylene glycol obtained by means of molecular dynamics simulations have been investigated and compared with the experimental data from positron annihilation lifetime spectroscopy (PALS). The results are also compared to those recently obtained on glycerol. The bulk microstructures of the samples have been analyzed in the temperature range 100–350 K with a probe-based procedure for exploring the free volume cavities of the microstructures. The basic free volume property, i.e., mean cavity volume, is compared with the hole volume data from PALS. A comparison between calculated and experimental data suggests the existence of a threshold volume for the smallest cavity detectable by PALS, which may be ascribed to fast local motions of the matrix constituents. At high temperatures the cavity analysis reveals the formation of an infinite cavity, i.e., percolation phenomenon. The onset temperatures of the percolation process in propylene glycol and glycerol are found to be close to the characteristic PALS temperature T_{b2}^{L}, where a pronounced change in the PALS response occurs, as well as to the characteristic dynamic Schönhals temperature T_{B}^{SCH}, and Stickel's temperature T_{B}^{ST}, marking a dramatic change in the primary α-relaxation properties.

Electronic supplementary material The online version of this article (doi:10.1007/s00214-007-0283-9) contains supplementary material, which is available to authorized users.

D. Račko · J. Bartoš
Polymer Institute, Slovak Academy of Sciences,
Dúbravská cesta 9, 842 36 Bratislava, Slovakia

R. Chelli (✉) · G. Cardini · S. Califano
Dipartimento di Chimica, Università di Firenze,
Via della Lastruccia 3, 50019 Sesto Fiorentino, Italy
e-mail: chelli@chim.unifi.it

D. Račko · R. Chelli · G. Cardini · S. Califano
European Laboratory of Non-linear Spectroscopy,
Via Nello Carrara 1, 50019 Sesto Fiorentino, Italy

1 Introduction

Supercooled liquid dynamics, and the closely related liquid to glass transition phenomenon, is a long-term topic of condensed matter physics. In the past decade, an important role of the so-called crossover effects in the supercooled liquids has been recognized [1]. These crossover effects are manifested by several empirical findings based mostly on relaxation results obtained by dielectric spectroscopy [1, 2] (DS). The first model-dependent analysis of the primary α-relaxation time, τ_α, over a wide temperature range proposed by Stickel revealed the presence of several dynamic regimes and the associated crossover DS temperatures T_{B}^{ST} and T_{A}^{ST} [3,4]. Recently, model independent analyses of the relaxation strength of the process, $\Delta\varepsilon_\alpha$ versus log τ_α, led to the finding of a dramatic change at the crossover Schönhals DS temperature, T_{B}^{SCH} close to T_{B}^{ST} [5]. A few explanations of these crossover phenomena have been proposed based on (1) the transition from a diffusion to an activated regime in the potential energy landscape [6], (2) cooperativity concept [5], (3) $T_{B}^{ST} \cong T_{0}^{CG}$ relationship, where T_{0}^{CG} is the dynamic crossover temperature of the extended free volume model [7], (4) a change in the strength of interparticle interactions expressed within the coupling model [8] and (5) a cage effect at the so-called critical temperature T_c of the mode coupling theory [2]. Recently, a further empirical signature of crossover effects has also been observed by one of us in the positron annihilation lifetime spectroscopy (PALS) response of a series of glass-forming liquids [9–12]. These characteristic PALS temperatures (T_{b1}^{L} and T_{b2}^{L}) correlate often with the abovementioned characteristic

DS temperatures via relationships: $T_B \approx 1.2T_g \approx T_{b1}^L$ [11], or sometimes $T_B \approx 1.2T_g \approx T_{b2}^L$ for small molecular van der Waals systems [10], or $T_B \approx 1.5T_g \approx T_{b2}^L$ in the case of small molecular hydrogen-bonded systems and polymers [9,12].

Recently we carried out a detailed atomistic modeling on glycerol [13] (GL) using molecular dynamics (MD) simulations followed by cavity analysis (CAVA) and found a dramatic change in the morphology of free space accessible to ortho-positronium (o-Ps) probe at the onset temperature commensurate with the characteristic PALS temperature T_{b2}^L. The aim of this paper is to present an analogous MD and CAVA study of a further glass-forming liquid, propylene glycol (PG), to verify the validity of the finding of the cavity percolation in the vicinity of the crossover temperature T_{b2}^L. A further confirmation to the hypothesis of the existence of a lowest limiting value for the cavity volume detectable by the o-Ps probe in PALS measurements is also provided.

2 Methods: molecular dynamics simulations and cavity analysis

The liquid and glassy microstructures of PG were generated by means of MD simulations using the ORAC program [14]. The same Lennard-Jones parameters used for GL [13] have been also adopted for PG, whereas the atomic charges were calculated as prescribed by the AMBER protocol [15] (see Table 1). A detailed description of the intramolecular and Lennard-Jones potentials is given in [16]. The samples consist of 300 molecules placed in a cubic box with standard periodic boundary conditions. The microstructures in the temperature range 100–350 K and 0.1 MPa were obtained by cooling down a sample equilibrated at 400 K. The cooling was performed by decreasing the temperature of the sample in steps of 10 K every 400 ps in the NPT ensemble (constant number of particles, constant pressure and constant temperature) employing the Andersen barostat [17] and the Nosé-Hoover thermostat [18]. The microstructures at each temperature were then equilibrated in the microcanonical (NVE) ensemble for 100 ps employing the average box dimensions obtained from the final 100 ps of the previous NPT runs. Then the atomic coordinates were stored during an NVE production run of 200 ps. In order to prevent the correlation between subsequent configurations, the structures for the CAVA were stored every 400 fs. The CAVA is carried out in two steps. At first, the free space regions of the sample are determined by inserting a spherical probe on the nodes of a three-dimensional grid covering the whole simulation box. The probe radius is set to 0.53 Å on the basis of a previous work [13], where the probe size effect has been tested and discussed. Only the probes that do not overlap with the molecules (whose volumes are determined on the basis of the van der Waals atomic radii) are considered to belong to a free space cavity. Next, the free space cavities are constructed, considering a cavity as an isolated set of overlapping probes. This procedure provides both the number of cavities in the sample and their corresponding volume. These two basic quantities allow the calculation of any other relevant free volume property, i.e., total free volume, mean cavity radius, mean cavity volume and free volume fraction, and the cavity volume distributions as well. More information on the algorithm used for the CAVA can be found in [13].

3 Results and discussion

The box volumes obtained via the NPT simulations are compared with experimental values as a function of temperature in Fig. 1. The experimental volumes were derived from dilatometric data of GL [19] and PG [20]. In the case of the experimental data, the temperature dependence can be approximated by two linear regions (at the low temperatures) determining the corresponding liquid–glass transition temperatures T_g. For the calculated data the change in slope of the curves is less evident and an accurate T_g cannot be distinguished visually. Therefore, for a better estimate of T_g, we use the number density of cavities as a function of temperature, i.e., the ratio between the total number of cavities and the volume of the simulation box (see supplementary material). The curve shows two well-defined linear regions whose intersection point determines T_g. In this way we estimate a T_g^{MD} of about 250 K for GL (see also Fig. 2 of [13]) and 230 K for PG (these values are also reported in Fig. 1). Overall the temperature dependence of the simulation box volume agrees well with the experimental data obtained from dilatometry [19,20]. The volume increases linearly with temperature in two distinct slopes. Its deviation from the experimental values for PG and GL is around 0.3% in the simulated liquid region and around 2.0% for PG and 1.3% for GL in the simulated glass. The larger difference between the experimental and the calculated values for the glassy samples arises from the fast cooling rate employed in the MD simulations.

Table 1 Electric charges (in electrons) for propylene glycol ($CH_3 - CHOH - CH_2OH$)

CH_3		CHOH		CH_2OH	
C	−0.393360	C	0.359201	C	0.111388
H	0.098500	Non-hydroxy H	−0.006198	Non-hydroxy H	0.034792
		O	−0.642605	O	−0.613930
		Hydroxy H	0.408209	Hydroxy H	0.412211

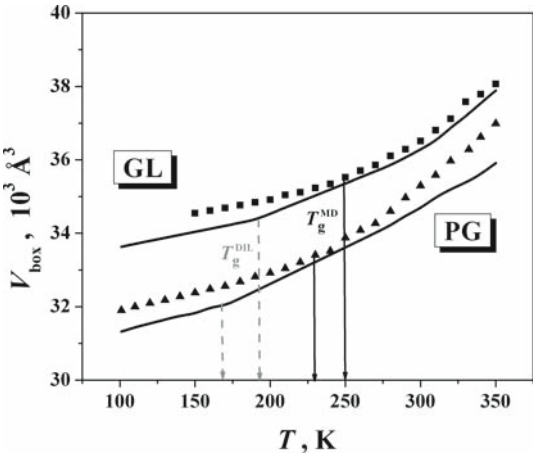

Fig. 1 Volume occupied by 300 molecules as a function of temperature. The calculated data for GL (*filled square*) and PG (*filled triangle*) are compared with dilatometric data (*solid lines*). The *arrows* show the calculated and experimental liquid–glass transition temperatures. The data on GL are taken from [13]

As a result, the simulated liquid–glass transition temperature is shifted to higher values reported above ($T_g^{MD} = 250$ K for GL and $T_g^{MD} = 230$ K for PG). These values are comparable with the T_g^{MD} estimates of 244 K for GL and 220 K for PG made on the basis of the cooling rate attained in our simulation study [13] using the Donth's formula [1], which is based on the experimental dilatometric liquid–glass transition temperature T_g^{DIL} [19,20] and on the fragility of the system [21]. In this respect we notice that, for a more correct quantitative comparison, T_g^{MD} should be determined by averaging over a large ensemble of cooling simulation processes, each starting from a different point of the phase space. This is essentially due to the small dimensions of the simulation samples with respect to the experimental ones that could make the reached glassy configuration, and hence T_g^{MD}, crucially dependent on the initial configuration of the system. Anyway, we may qualitatively conclude that, due to the fast cooling rate, the microstructures are frozen at higher amounts of free volume causing a significantly worse reproduction of the experimental volumes below the simulated liquid–glass transition temperature.

In the following the calculated mean cavity volumes and mean cavity radii are compared with the experimental mean hole volumes and radii, respectively. Figure 2 shows the calculated mean cavity volume (thick solid lines) as a function of temperature. The mean cavity volume is calculated by including all cavities according to the obvious definition, i.e., the total cavity volume divided by the total number of cavities [22]. From an experimental point of view, a properly defined mean cavity volume cannot actually be determined. Instead, from PALS measurements the mean free volume hole radius is available via a quantum-mechanical model of o-Ps lifetime in a spherical hole [23–25]. Following this

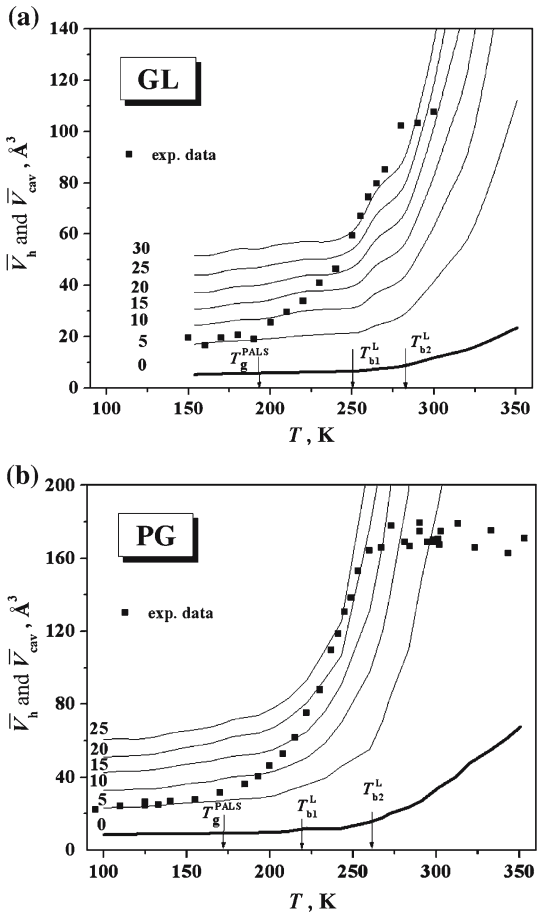

Fig. 2 Calculated mean cavity volumes as a function of temperature for PG and GL. The calculation performed without any assumption on the threshold volume for the smallest cavity ($V_{lim} = 0$) is reported with *thick solid lines*. The mean cavity volume calculated using different threshold volumes ($V_{lim} = 5$, 10, 15, 20, 25 and 30 Å^3) for the smallest cavity are reported with *thin solid lines*. The experimental mean hole volumes for PG [26] and GL [9] are shown with *symbols*. The *arrows* mark the characteristic PALS temperatures. The data on GL are taken from [13]

model, the o-Ps lifetime τ_3 can be expressed in terms of geometrical parameters:

$$\tau_3 = \frac{1}{2}\left[1 - \frac{R_h}{R_h + \Delta R} + \frac{1}{2\pi}\sin\left(\frac{2\pi R_h}{R_h + \Delta R}\right)\right]^{-1} \quad (1)$$

where R_h is the mean hole radius and $\Delta R = 1.656$ Å is the thickness of the electron layer around the hole. ΔR has been determined by fitting τ_3 for systems of known hole size (zeolites and molecular crystals) using Eq. 1. From R_h evaluated using Eq. 1, we can obtain the so-called mean hole volume[1] through the simple relation $\bar{V}_h = {}^{4\pi}/_{3} R_h^3$. Note that, as the *real* free volume holes are generally non-spherical,

[1] The use of a different name for the *mean hole volume* with respect to the *mean cavity volume* (used for the calculated analogous quantity) stresses the different procedures employed for determining such quantities.

the quantities R_h and $\bar{V}_h$ are intended as an *equivalent* mean radius and a corresponding mean volume. The experimental mean hole volume of PG [26] and GL [9] is also shown in Fig. 2. As we can see from the figure, the mean cavity volume is significantly smaller than the mean hole volume for PG and GL systems. This result is actually important because it strongly supports the findings obtained recently on GL [13]. On the basis of the very large difference between experiment and calculation in terms of mean hole/cavity volume, well beyond the difference observed in the total volume (Fig. 1), we may conclude that some physical effect must occur in the reality that is not accounted for in the MD/CAVA modeling. The systematic large deviation of these calculated and experimental quantities requires an introduction of a limiting accessible cavity volume [13,27]. This concept postulates the existence of a smallest limiting cavity volume, V_{lim}, inaccessible to the o-Ps probe localization due to small-scale high-frequency motions [13,27]. Taking V_{lim} into account, the mean cavity volume can be calculated as follows:

$$\bar{V}_{cav} = \frac{\int_{V_{lim}}^{\infty} V\, N(V)\, dV}{\int_{V_{lim}}^{\infty} N(V)\, dV} \tag{2}$$

where $N(V)$ is the number of cavities having volume V. The mean cavity volume calculated with various V_{lim} values is shown in Fig. 2. The largest portions of small cavities occur at low temperature and disappear with increasing temperature when the free space is localized in large cavities. The exclusion of these small cavities enhances the bending of the mean cavity volume versus temperature dependence resulting in the typical curvature observed for the experimental mean hole volumes. From the comparison between calculated mean cavity volumes and experimental mean hole volumes in the temperature range above T_g^{MD} and below T_{b2}^{L} (the range is 230–265 K for PG and 250–285 K for GL), we estimate the limiting volume of the smallest detectable cavity to be 25 and 30 Å^3 for PG and GL, respectively. As yet the T_{b2}^{L} temperature represents an intrinsic limit of the PALS applicability above which the experimental temperature dependence of the mean hole volume declines to a plateau. For PG, the mean volume of the cavities, whose volume is lower than the threshold value V_{lim} of 25 Å^3, is 3.6 Å^3. This volume corresponds to an equivalent spherical radius of 0.95 Å. For GL, the mean volume of the cavities below the threshold value V_{lim} of 30 Å^3 and the equivalent spherical radius are 3.8 Å^3 and 0.97 Å, respectively.

The comparison between mean cavity volume and mean hole volume reported in Fig. 2 provides clear qualitative insights into the possible mechanisms (smallest detectable cavity) underlying PALS measurements. However, as stated above, a quantitative comparison would be at least improper, because the MD derived quantity is obtained from an average over all cavity volumes, whereas the mean hole volume results from an a posteriori manipulation of the mean cavity radius determined from Eq. 1. In order to quantitatively assess the difference between calculated and experimental data, we have thus calculated the mean cavity radius from MD simulations, whose determination from the knowledge of the sample configurations is straightforward: for each cavity volume evaluated as described in Sect. 2, we have estimated the equivalent spherical radius and then averaged over all cavities of the microstructures. Figure 3 shows the comparison between the calculated and the experimental mean cavity radii as a function of the temperature, for both GL and PG. The best match between experimental and calculated curves is obtained for $V_{lim} = 40$ Å^3, which is larger than that recovered by comparing the cavity volumes (see above and Fig. 2). The larger eliminated volume is the result of the decreased weight of the large cavities in the system by the third root of their volumes. The mean radius of the eliminated cavities for PG and GL is nearly the same, i.e., 1.0 Å. The information retrieved from the comparison of the calculated and experimental mean cavity radii is thus consistent, even from the quantitative point of view, with the results for the mean cavity volume and mean hole volume discussed above.

The integral distributions of the free volume fraction in the simulated microstructures as a function of the free cavity volume, V_{cav}, are calculated using the following equation:

$$I(V_{cav}) = \frac{\int_0^{V_{cav}} V\, N(V)\, dV}{\int_0^{\infty} V\, N(V)\, dV} \tag{3}$$

where $N(V)$ has been defined above (see Eq. 2). Figure 4 shows the integral distributions calculated for several

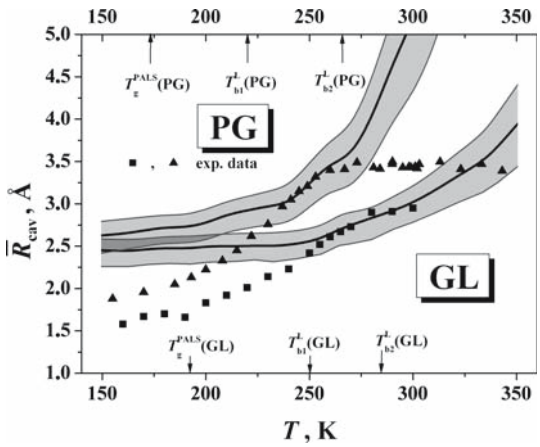

Fig. 3 Calculated and experimental mean cavity radius as a function of temperature for PG and GL. The calculated mean cavity radius (*solid lines*) has been obtained using $V_{lim} = 40$ Å^3. The *bottom* and *upper borders* of the gray areas correspond to $V_{lim} = 30$ Å^3 and $V_{lim} = 50$ Å^3, respectively. The experimental data for GL [9] and PG [26] are shown with *squares* and *triangles*, respectively. The *arrows* show the characteristic PALS temperatures. The data on GL are taken from [13]

temperatures from glassy to supercooled liquid and liquid phases for both systems, PG and GL. The curves below the simulated liquid–glass transition are almost temperature independent, consistent with frozen free volume microstructures. Upon increasing the temperature, the free volume localizes into larger and larger cavities, accompanied by an almost discontinuous path on the integral distribution curves. The formation of a fully percolated cavity (periodic boundary crossover) can be indicated within the cavity construction procedure [13] and it is shown graphically in Fig. 5 for PG at three temperatures. For GL, such representation was reported in [28]. The formation of a very large cavity at high temperature, extending over the whole simulation sample, appears evident. From Fig. 4 we see that the free volume cavities give rise to rather large distribution widths in the case of low temperatures (smooth increase of the integral distribution means broad free volume cavity distribution, while a rapid increase corresponds to a narrow distribution). On the other hand, such widths become very narrow at higher temperatures (T > 300 K for PG and T > 330 K for GL), suggesting the existence of simulation artifacts. Naturally this effect is to be ascribed to the finite size of the simulation box that imposes an upper limit to the cavity dimension. Thus the presence of the percolation cavity due to the periodic boundary leads to an underestimate of true cavity size in absolute numbers. The estimate of the true cavity-size distribution would require employment of a larger simulation box. Although such an investigation is possible, it does not add any new significant insights to our qualitative conclusions.

The onset of the cavity percolation in the microstructures is observed at around 300 K for GL and 250 K for PG. An extensive percolation of the whole free volume is indicated by a shoulder on the integral distributions approximately 30 K above the first percolated cavities appear. The temperatures to which cavity percolation appears (see above) are comparable to the characteristic PALS temperature T_{b2}^{L} (which is around 280–290 K for GL [9] and 265 K for PG [26]; see also Fig. 2) as well as to the characteristic DS temperatures ($T_B^{ST} = 287$ K for GL [4] and $T_B^{SCH} = 268$ K for PG [5]). Moreover, an equivalence between the o-Ps lifetime τ_3 and the α-relaxation time τ_α is observed at $T = T_{b2}^{L} \cong T_B^{ST} \cong T_B^{SCH}$, whereas for $T < T_{b2}^{L}$ and $T > T_{b2}^{L}$ the relationships $\tau_3 < \tau_\alpha$ and $\tau_3 > \tau_\alpha$ hold, respectively [9,11]. All these facts lead to the formulation of a concept of dynamic free volume facility. In other words, the presence of percolated free volume cavities makes easier or facilitates a qualitative change in the primary α-relaxation. As mentioned in Sect. 1, the crossover effect in the dynamic properties is explained in terms of decrease in "the extent of cooperativity" according to Schönhals' idea [5] or by a decrease in "the strength of interparticle interactions" according to Casalini et al. [8]. Our study on PG indicates that the crossover phenomenon in the PALS response can stem from the mutual interplay between

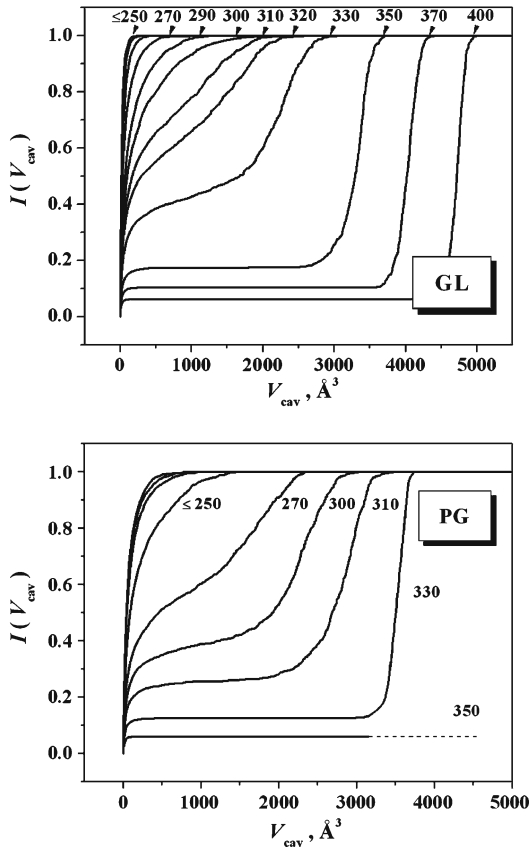

Fig. 4 Integral distributions of the free volume into cavities, calculated by means of Eq. (3), for PG and GL at various temperatures (*numbers* on the graphs). The data on GL are taken from [13]

the increasing empty free space associated with the occurrence of percolating cavity volume (which clearly brings an increase in the o-Ps lifetime) and the increasing dynamic rearrangement of particle constituents of the matrix (which could give rise to a decrease of the o-Ps lifetime). Thus, this analysis is consistent with the changes in the dynamic relaxation properties as well as with the so far proposed interpretations.

4 Conclusions

We have investigated the free volume microstructures of propylene glycol by means of MD simulations and compared the data to those recently reported on glassy and liquid glycerol. The free volume analysis has been performed in the temperature range 100–350 K on a total of 2.5×10^4 microstructures. The comparison of the computed data with the experimental mean hole volumes obtained from the positron annihilation lifetime spectroscopy allowed us to address several phenomena with dynamical origin. The existence of a smallest detectable cavity is qualitatively consistent with small-scale high-frequency motions restricting the cavities

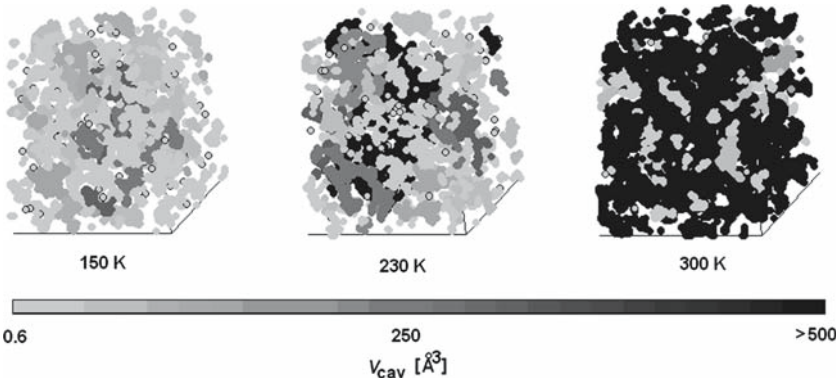

Fig. 5 Three-dimensional view of free volume microstructures for three representative temperatures for PG. The size of the cavities (V_{cav}) is indicated by intensity of shading according to the scale. The cavities with volume of exactly one probe are distinguished by *circles*. With increasing the temperature, the free volume situates in larger cavities. The number of small cavities decreases while they join the larger ones. At high temperatures the free volume is situated mostly in one cavity only, which percolates the periodic box through its boundaries

for o-Ps localization. Our finding on the percolation of the cavity volume, observed at high temperature near the characteristic dielectric T_B^{ST} and T_B^{SCH} temperatures, is consistent with the current interpretations of dynamic processes involving the decrease in the extent of cooperativity and in the strength of interparticle interactions above these crossover temperatures.

Acknowledgments This work was supported by the NSF Grant No. 0217129, USA, the VEGA Grant No. 2/6035/26, Slovakia, the APVT Grant No. 51- 045302, Slovakia and the European Union Grant No. RII3-CT-2003-506350.

References

1. Donth E (2000) The Glass Transition, Springer, Berlin
2. Adichtchev S, Blochowicz T, Tschirwitz C, Novikov VN, Rössler EA (2003) Phys Rev E 68:011504
3. Stickel F, Fischer EW, Richert R (1996) J Chem. Phys 102:6251
4. Stickel F (1995) PhD Thesis, Shaker Verlag Aachen
5. Schönhals A (2001) Europhys Lett 56:815
6. Goldstein M (1969) J Chem Phys 51:3728
7. Paluch M, Casalini R, Roland M (2003) Phys Rev. E 67:021508
8. Casalini R, Ngai KL, Roland CM (2003) Phys Rev B 68:014201
9. Bartoš J, Šauša O, Krištiak J, Blochowicz T, Rössler E (2001) J Phys Cond Matt 13:11473
10. Ngai KL, Bao LR, Yee AF, Soles ChL Yee (2001) Phys Rev Lett 87:215901
11. Bartoš J, Šauša O, Bandžuch P, Zrubcová J, Krištiak J, Non-Cryst J (2002) Solids 307–310:417
12. Bendler JT, Fontanella JJ, Shlesinger MF, Bartoš J, Šauša O, Krištiak J (2005) Phys Rev E 71:0315089
13. Račko D, Chelli R, Cardini G, Bartoš J, Califano S (2005) Eur Phys J D 32:289
14. Procacci P, Darden TA, Paci E, Marchi M (1997) J Comput Chem 18:1848
15. Cornell WD, Cieplak P, Bayly CI, Gould IR, Merz KM Jr., Ferguson DM, Spellmeyer DC, Fox T, Caldwell JW, Kollman PA (1995) J Am Chem Soc 117:5179
16. Chelli R, Procacci P, Cardini G, Della Valle RG, Califano S (1999) Phys Chem Chem Phys 1:871 (The σ parameters of the Lennard-Jones potential reported in Table 1 are wrong. The correct values are: 3.4, 3.0665 and 2.4713 Å for the atoms C, O and non-hydroxy H, respectively)
17. Andersen HC (1980) J Chem Phys 72:2384
18. Hoover WG (1985) Phys Rev A 31:1695; Hoover WG (1986) Phys Rev A 34:2499
19. Kovacs AJ (1964) Fortschr Hochpolym-Forsch 3:394
20. Parks GS, Huffman HM (1927) J Chem Phys 31:184
21. Beiner M, Huth H, Schröter K (2001) J Noncryst Sol 279:126
22. Sastry S, Truskett TM, Debenedetti G, Torquato S, Stillinger FH (1998) Mol Phys 95:289
23. Tao SJ (1972) J Chem Phys 56:5499
24. Eldrup M, Lightbody D, Sherwood JN (1981) Chem Phys 63:51
25. Nakanishi H, Wang SJ, Jean YC (1988) In: Sharma SC (ed) Positron annihilation studies of fluids. World Scientific, Singapore p 292
26. Bartoš J, Šauša O, Krištiak J (in press)
27. Bartoš J, Šauša O, Račko D, Krištiak J, Fontanella JJ (2005) J Noncryst Solids 351:2599
28. Bartoš J, Račko D, Šauša O, Krištiak J (2007) Positron annihilation lifetime spectroscopy and atomistic modeling—effective tools for the disordered condensed system characterization, ARW NATO Series. Springer, Berlin, p 110